The Development of a Volume-of-Fluid Interface Tracking Method for Modeling Problems in Mantle Convection

Jonathan Robey[1]

August 27, 2016

[1]Funded in part by a GAANN Fellowship

1 Summary

In problems involving mantle convection, it is often important to track the movement of a conserved fluid or material volume. Although in some cases this can be done by modeling the advection equation for a compositional variable, often the smearing/diffusion introduced by standard numerical methods for modeling the advection equation obscures or eliminates essential information, such as the material interface. In our work, we implement a Volume-of-Fluid (VoF) interface tracking method in a large open source finite element code, ASPECT [4], for modeling convection in the Earth's mantle.

In section 2 we briefly discuss the applications of our method to geodynamic problems. In section 3, the we describe the equations governing convection in the Earth's mantle and the numerical methodology we use to model them. In section 4, we describe in detail the VoF methodology. In section 5, we present numerical results including computations to validate the accuracy of the newly implemented VoF algorithm in ASPECT and show applications of this new algorithm to a problems in mantle convection. In section 6, we discuss future directions for this work.

2 Geodynamics Background

Mantle convection is one of the primary areas of interest in the field of geodynamics. Due to the nature of the problem, computational modeling is an essential tool for examining wide variety of problems that are associated with mantle convection. The underlying problem, thermally driven convection (i.e. the Rayleigh-Bernard equations), is well established problem in fluid dynamics. In a number of situations the ability to carefully track a fluid or material volume is highly desirable, due to variations in fluid properties or interest in location of the fluid interface. This suggests the use of an interface tracking method.

3 Computational Background

3.1 Introduction

Over the past forty years, a number of codes have been developed for the purpose of modeling convection in the Earth's mantle. ASPECT, a finite element code designed for extensibility, is currently among the best codes in the field. However, it does not have any interface tracking ability, other than with tracer particles. Furthermore, to the best of our knowledge no other state-of-the-art mantle convection codes have interface tracking capability. Thus, the addition of a VoF interface tracking extension to ASPECT will be of significant value to researchers in the mantle convection community.

The VoF method is an interface tracking algorithm designed to use the advection of an indicator or 'color' function to approximate the location of the interface between two fluid volumes. The core of the method is similar to a

finite volume advection scheme, though specialized for to tracking the interface of an indicator or color function. As such, VoF methods are inherently conservative; i.e. their basic design will conserve the material being tracked.

3.2 An Overview of Current Interface Tracking Methods

In this section we discuss a general overview of several standard interface tracking methods.

The interface tracking problem is found in a wide variety of applications in science and technology, and as such a number of approaches to modeling the motion of an interface have been proposed. As with many numerical solutions to PDEs, it is first necessary to choose between Eulerian and Lagrangian approaches. In a number of ways, the Lagrangian approach is the more intuitive for the interface problem, but is subject to many difficulties especially in cases where the interface distorts or fragments. While it is possible to find solutions to these issues, the most robust solutions frequently require significant computational resources in addition to presenting complex algorithmic issues. For these reasons, an Eulerian approach is frequently the better choice.

The simplest Eulerian approach is to use a continuous approximation of the indicator function. However, this has the interface smearing/diffusion issue mentioned earlier. For this reason, it is often better to employ an interface tracking algorithm, which provide the user with sub-grid resolution of the material interface.

One Eulerian interface tracking algorithm is the level set method[9], in which the interface is given by the zero contour of smooth function ϕ. This generates a sharp boundary. However for problems such as the ones we are interested in one must solve a Hamilton-Jacobi equation to advance the location of the interface. This requires a complex set of methodologies, originally developed for modeling shock waves such as limiters and entropy conditions. This is still an active area of research in the finite element community. Additionally, this approach does not inherently conserve volume, since the level set function ϕ is not a conserved quantity.

Another Eulerian approach is the VoF method. Like the level set method, the VoF method has as a primary goal of maintaining a sharp interface between the two fluids. In the case of the VoF method this is done using volume fraction data f_i, and then reconstructing the fluid interface on a sub-grid level in each cell of the mesh where $0 < f_i < 1$. The interface reconstruction step only requires access to the volume fraction in neighboring cells, and as such is inherently parallelizable.

3.3 Equations

The equations solved by Aspect for the velocity field are the incompressible Stokes equations, given below in equation 1, where $\vec{f}(\vec{x},t)$ is the body force, in this case gravity. In this equation, P is pressure, μ is viscosity, $\vec{u} = (u,v)$ is the velocity vector, and ρ is density. The temperature is handled using the

standard advection-diffusion equation as given in equation 2. Here k is the thermal conductivity and c_p is the specific heat at constant pressure. Any continuous composition fields C are handled using the advection equation as given in equation 3. The composition field that we wish to maintain a sharp interface on using an interface tracking scheme is to be propagated using the VoF method, which will be described in more detail below.

$$-\frac{\partial P}{\partial x} + \mu\left(\frac{\partial^2 u}{\partial x^2} + \frac{\partial^2 u}{\partial y^2}\right) = \rho\vec{e}_x \cdot \vec{f}(\vec{x}, t) \tag{1a}$$

$$-\frac{\partial P}{\partial y} + \mu\left(\frac{\partial^2 v}{\partial x^2} + \frac{\partial^2 v}{\partial y^2}\right) = \rho\vec{e}_y \cdot \vec{f}(\vec{x}, t) \tag{1b}$$

$$\nabla \cdot \vec{u} = 0 \tag{1c}$$

$$\frac{\partial T}{\partial t} + \vec{u} \cdot \nabla T = \frac{k}{\rho c}\Delta T \tag{2}$$

$$\frac{\partial C}{\partial t} + \vec{u} \cdot \nabla C = 0 \tag{3}$$

For the velocity solution, the Boussinesq approximation is used to close the equations.

$$\rho(T) = \rho_0(1 - \alpha_v(T - T_{ref})) \tag{4}$$

This particular approximation combines the incompressible Stokes equations with a buoyancy force based on a density variation which is linear in temperature. The relevant velocity field equations are then given by [from 10]

$$-\frac{\partial P}{\partial x} + \mu\left(\frac{\partial^2 u}{\partial x^2} + \frac{\partial^2 u}{\partial y^2}\right) = 0 \tag{5a}$$

$$-\frac{\partial P}{\partial y} + \mu\left(\frac{\partial^2 v}{\partial x^2} + \frac{\partial^2 v}{\partial y^2}\right) = g\rho_0\alpha_\nu(T - T_0) \tag{5b}$$

$$\nabla \cdot \vec{u} = 0 \tag{5c}$$

Like standard advection equation schemes, the VoF method begins with the integral form of the standard fluid advection equation (6) where Ω_i denotes a grid cell.

$$\frac{d}{dt}\int_{\Omega_i} \Phi(\vec{x}, t)d\vec{x} + \int_{\Omega_i} \vec{u} \cdot \nabla\Phi(\vec{x}, t)d\vec{x} = 0 \tag{6}$$

At this point standard methods assume a continuous approximation $f(\vec{x}, t)$ of Φ allowing a reduction to a pointwise limit and obtain a differential equation from that. By contrast, VoF methods track $f_i = \int_{\Omega_i} \Phi(\vec{x}, t)d\vec{x}$, and continue

from the integral form by making use of the additional constraint that Φ is an indicator function in order to reconstruct an approximation to the true interface. The reconstruction does require the assumption of some minimum length scale for features of interest, and for pure VoF methods also depend on surrounding cell volumes. The resultant approximation to the true interface Φ^* then does not include any of the numerical smearing that would occur for standard advection methods, so the interface remains localized to a single cell.

To obtain the new state values $\{f_i^{n+1}\}$ from $\{f_i^n\}$, the divergence theorem is applied to the integral form 6. Letting $f_i^n = \int\limits_{\Omega_i} f(\vec{x}, t^n) d\vec{x}$, this is then integrated over time to obtain the equation

$$f_i^{n+1} = f_i^n + \int\limits_{t^n}^{t^{n+1}} \int\limits_{\Omega_i} f \nabla \cdot \vec{u} d\vec{x} dt - \int\limits_{t^n}^{t^{n+1}} \int\limits_{\partial\Omega_i} f \vec{u} \cdot \vec{n} d\vec{x} dt \tag{7}$$

This can then be discretized using average values computed from the finite element solution for $\nabla \cdot \vec{u}$ and $\vec{u} \cdot \vec{n}$, while using a method of characteristics based approach to find the donor region that is then used to compute the volume fractions on the apertures ($\partial\Omega_i \mathrm{x} [t^n, t^{n+1}]$). For the incompressible Stokes equations $\nabla \cdot \vec{u} = 0$ and normally we can assume that this term may be dropped. However, for some volume fraction update algorithms, such as a dimensionally split approach, the effective velocity field during the update step may not remain divergence free and therefore the term is retained.

This discretization of equation 7 is equivalent to a Discontinuous Galerkin method with zeroth order elements and a specialized flux term computation or equivalently to a standard finite volume method. As such, the method can be included in the Finite Element code ASPECT without requiring significant logic to translate between assumptions.

4 Computational Approach

4.1 Implementation

The necessary finite element matrix assembler and solver for the Boussinesq approximation have already been implemented as part of ASPECT. It is therefore sufficient to consider only the implementation of the volume of fluid method, and the means by which any information necessary to the main algorithm may be provided to the velocity computation.

To implement the VoF method, it is necessary to select both a a suitable interface reconstruction method and an algorithm for advecting the volume fractions based on the reconstructed interface and the computed velocity field.

For the interface reconstruction algorithm, we use the Efficient Least-Squares VoF algorithm (ELVIRA) developed by Pilliod [5] and Pilliod and Puckett [6] due to ease of implementation, low computational cost, and second-order accuracy. The algorithm is a modification of the full iterative least-squares interface

reconstruction method [7] that selects between a short list of candidates shown to include the true interface for a linear interface, or a second order approximation for general interfaces given the eight surrounding cells and a maximum interface curvature. To ensure that linear interfaces are reproduced exactly for cells on the edge of the mesh, the normal direction of the interface in the cell at the past timestep is appended to the list of candidates. In the cases where this addition has any effect, it will result in the selected normal direction being closer to that generated by the more accurate least-squares algorithm specified by Puckett [7].

The piecewise linear interface algorithm ELVIRA constructs interfaces of the form $\vec{n} \cdot \vec{x} = d$ for each cell, with d chosen such that the volume enclosed in the cell is equivalent to the current volume fraction. For application to the finite element mesh generated for ASPECT, this was modified to be $\vec{n} \cdot \hat{x} = d$ where $\hat{x}$ is the coordinates for a standard unit cell.

This algorithm requires the computation of the volume fraction or interface location given the other quantity and a particular normal vector rather frequently. Due to the chosen method of computation, which makes use of the same relation between the two for the two-dimensional case noted by Scardovelli and Zaleski [8], the current implementation is limited to a parallelogram mesh. Acceptance of this implmentation greatly reduces the required complexity of the code for the moment and can also be expected to significantly reduce the computational cost. Generalizing to permit more freedom in mappings is likely to necessitate an iterative scheme for computing the appropriate d given a volume fraction f, which can be expected to significantly increase the computational cost of the algorithm. See section 6 'Future Work'.

In order to simplify the flux fraction calculation, one standard approach for VoF methods is to use a dimensionally split algorithm with appropriate designations for the donor regions. This does require some additional consideration of the method of handling the divergences in the split velocity field as discussed in section 3.3. The particular method chosen in the case of this implementation is to include the divergence term for the advection calculation with an implicit discretization of the volume fraction for said term, ensuring that the volume fraction remains bounded within $[0, 1]$.

The final implementation problem is how to provide the VoF data to the main solver. In order to best make use of the existing solver infrastructure, the volume of fluid data is used to generate a finite element composition field approximation to the color function that is then used in the standard manner by the velocity equation solver. The problem is then to select the appropriate means of making this approximation. Use of a discontinuous galerkin finite element permits the approximation to be local to cell of interest. Considering the relative structural scales and configurations, it was decided that polynomial elements of degree 1 would be most reasonable for both ease of calculating the approximation and not reaching beyond the level of information available. It is possible to generate simple interpolations that satisfy any two of the obvious criteria of bounded on $[0, 1]$, volume fraction preserving, and that the fluid interface be at $C(\vec{x}) = 0.5$, but attempting to satisfy all three of these is not

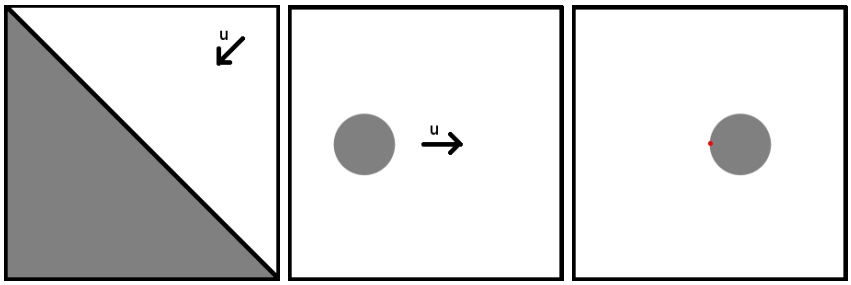

(a) Linear interface translation problem

(b) Circular interface translation problem

(c) Circular interface rotation problem, red dot is center of rotation

Figure 1: Sketches of rate of convergence tests

possible with the given discretization. Considering the case for minimum L^2 error for a linear mapping and a P_{-1} element, the requirements generated are that both volume fraction and fluid moment match for the true interface and the approximation. This suggests that the correct approach is to use the first two criteria.

5 Results

5.1 Validation

In order to ensure that the implementation of the interface tracking method is second-order accurate for smooth interfaces, we tested it on several problems advecting a known interface under a prescribed velocity field.

These tests require a method by which to approximate the error of the VoF method. The obvious approach is to consider the volume where the approximate and exact interfaces differ. However, even for linear interfaces the calculation of this quantity is not simple, and useful test cases cannot all have linear interfaces everywhere.

As such, an approximation by quadrature is necessary, and the use of a continuous approximation to the Heaviside function is likely to produce more useful information. In order to select a reasonable approximation, we begin by noting that the use of an iterated midpoint quadrature could equivalently be describe as evaluating the differences in volume fractions on given subregions of the cell with the volume fractions specified only by the type of fluid at the cell center. When considered in this manner, an obvious improvement is to do the volume fraction estimation by using linear approximations to the interfaces on the given volumes, which results in a C^1 function (C^2 almost everywhere) which differs from the Heaviside function only in regions within $\frac{\tilde{h}\sqrt{2}}{2}$ of the interface where $\tilde{h}$ is the width of a subregion. Examination of the various cases shows that on volumes with non-disjoint fluid volumes and linear non-intersecting interfaces

this is exact. This approximation will be reported in tables as the 'L1 Interface Error'.

Another approach to error estimation is to make use of the initialization procedure to generate the 'correct' volume fractions for the discretization at a given time, and then do a standard ℓ_1 norm of the difference between the the correct and computed volume fractions. This approach does not take into consideration the current interface reconstruction, since it only measures the difference in the current volume fractions. This error measurement will be referred to as the 'L1 Field Error'.

Both error measurements are normalized by the correct interface length. This value can then be intuitively considered as the average distance from the correct interface.

k	L1 Interface Error	L1 Field Error
4	$1.27552 \cdot 10^{-16}$	$1.32630 \cdot 10^{-16}$
5	$2.75932 \cdot 10^{-16}$	$2.74613 \cdot 10^{-16}$
6	$4.69302 \cdot 10^{-16}$	$4.69034 \cdot 10^{-16}$
7	$1.19555 \cdot 10^{-15}$	$1.19552 \cdot 10^{-15}$
8	$2.02016 \cdot 10^{-15}$	$2.01992 \cdot 10^{-15}$

Table 1: Error after translation in $[0,1]^2$ of the linear interface $y = 1 - x$ in the constant velocity field $\vec{u} = (-\frac{1}{4}, -\frac{1}{4})$ for 1 time unit, sketch is in figure 1a

First, the implementation was confirmed to reproduce linear interfaces under constant velocity fields to within machine epsilon (figure 1a). Due to the lack of sufficient bordering cells near the boundaries, an exact reproduction did, as expected, require the previously mentioned addition of an extrapolation of the past interface normal to the reconstruction candidate normals. The particular error values for the test are given in table 1, and are all on the order of machine epsilon. Though the reported error is growing, inspection suggests that it is likely due to accumulation of machine precision subtraction errors over the entirety of the mesh, which is likewise increasing in size.

The second, and more complex validation problem was translation of a circular interface under a constant mesh-aligned velocity field (figure 1b). In particular, using the domain $[-2,2]^2$, a circular interface of radius $\frac{1}{2}$ centered at $(-1,0)$ was advected under the velocity field $\vec{u} = (1,0)$ for two time units under varying CFL numbers. The results of this test are given in table 2. For CFL $\sigma = 1$, we observe the expected design convergence rate of 2 where the advection error can be expected to be minimal.

Finally, the algorithm was tested on advecting a circular interface (figure 1c). In particular, the test problem advects a circular interface of radius $\frac{1}{8}$ centered at $(\frac{1}{8}, 0)$ in the region $[-\frac{1}{2}, \frac{1}{2}]^2$ under the velocity field $\vec{u} = \pi(-y, x)$. The results of this test are given in table 3. Again, the observed convergence rate is second-order.

CFL $\sigma = 1$

k	L1 Interface Error	Rate	L1 Field Error	Rate
5	$1.89618 \cdot 10^{-3}$		$1.26228 \cdot 10^{-3}$	
6	$3.82585 \cdot 10^{-4}$	2.31	$2.36274 \cdot 10^{-4}$	2.42
7	$9.07219 \cdot 10^{-5}$	2.08	$3.31707 \cdot 10^{-5}$	2.83
8	$2.07321 \cdot 10^{-5}$	2.13	$6.34625 \cdot 10^{-6}$	2.39

Table 2: Error after mesh-aligned constant velocity field translation of a circular interface for two diameters, sketch in figure 1b

k	L1 Interface Error	Rate	L1 Field Error	Rate
4	$8.08431 \cdot 10^{-3}$		$8.08431 \cdot 10^{-3}$	
5	$2.35671 \cdot 10^{-3}$	1.78	$2.33441 \cdot 10^{-3}$	1.79
6	$5.27489 \cdot 10^{-4}$	2.16	$5.23932 \cdot 10^{-4}$	2.16
7	$1.41767 \cdot 10^{-4}$	1.90	$1.40612 \cdot 10^{-4}$	1.90
8	$3.52731 \cdot 10^{-5}$	2.01	$3.50275 \cdot 10^{-5}$	2.01

Table 3: Error after 1 full rotation of a circular interface offset from center of rotation by 1 Radius, sketch in figure 1c

5.2 Application

In this section, we present three computations of problems that are relevant to those that arise in mantle convection. The first two are a standard benchmarks in the field, and the third is directly related to an active research project I am engaged in with Professors Turcotte, Billen, and Kellogg in the departmen of Earth and Planetary Sciences.

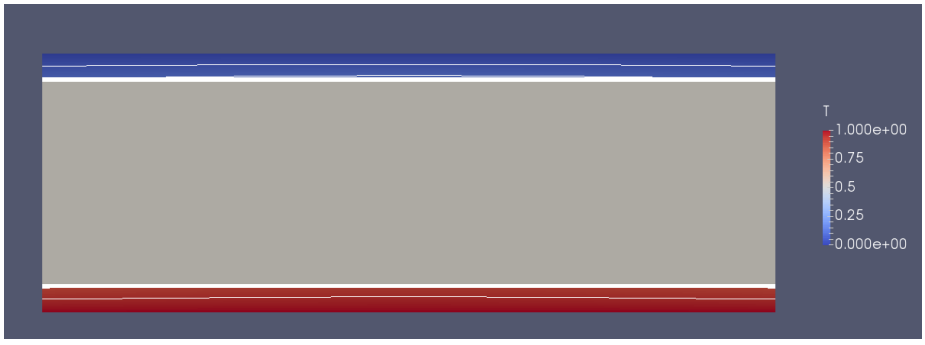

Figure 2: Contour and colormap for initial temperature as generated on a 192x64 mesh

For the first problem the newly implemented VoF method is used to track the uppermost 10% of the fluid volume under the following initial conditions. The values used for the relevant constants are $\rho_0 = 1$, $c_p = 1$, $T_{ref} = 0.5$, $k = 10^{-5}$, $\alpha_v = 10^{-4}$, and $\mu = 10^{-3}$ for a Rayleigh constant of $R_a = 10^5$. The domain is $[-\pi, \pi]x[0, 1]$ so $d = 1$ and $L = 2\pi$ with free-slip and no flow velocity boundary conditions. The temperature boundary condition are zero Neumann for the left and right boundaries, and the top and bottom use constant temperature boundary conditions of $T_0 = 0$ and $T_1 = 1$ respectively. The temperature was then initialized with perturbation amplitude $A = 0.05$ to the function given in equation 8, which is also shown as a colormap and superimposed contour plot in figure 2.

$$T(x, y, 0) = \begin{cases} T_0 + T_1(1 - \frac{y}{d}) + A\sin(\frac{y\pi}{d})\cos(\frac{x\pi}{L}) & y > \frac{9d}{10} \text{ or } y < \frac{d}{10} \\ T_{ref} & \text{otherwise} \end{cases} \tag{8}$$

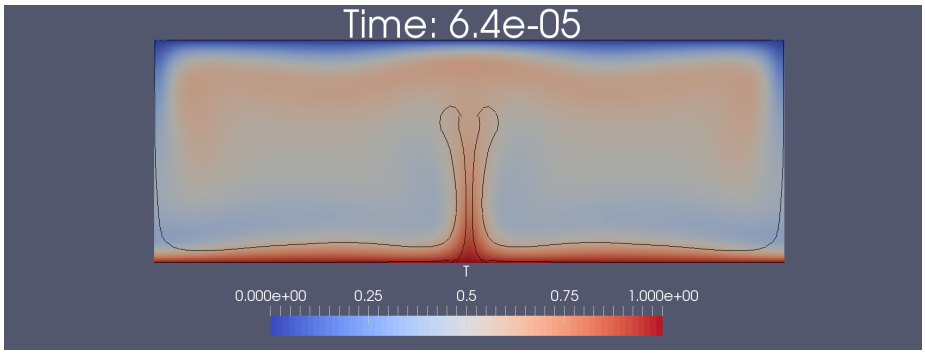

(a) Uniform 96x32 mesh

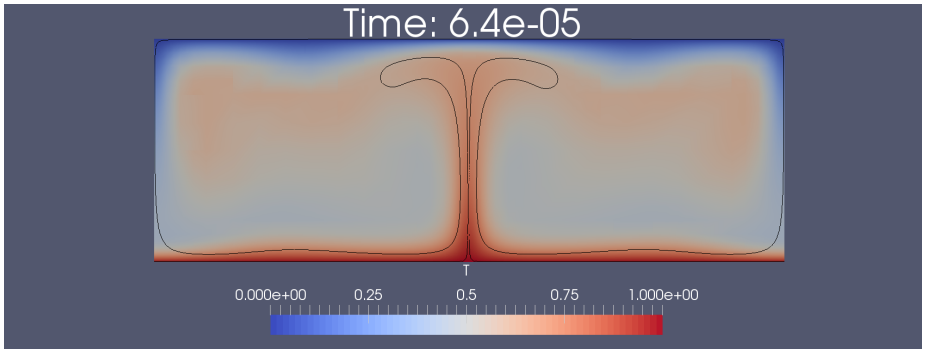

(b) AMR mesh with maximum resolution 384x128

Figure 3: Fluid state for $R_a = 10^5$ convection problem

The results for a uniform 192x64 mesh are shown in figure 3a. The general structure of the fluid interfaces observed matches that described by Turcotte [10]

for simple convection rolls. The result of using a AMR refinement scheme to obtain a slightly higher resolution is given in figure 3b. The contrast between the two interfaces is likely due to a better resolution of the initial temperature in the AMR version adjusting the velocity field and thus the length of the initial timesteps.

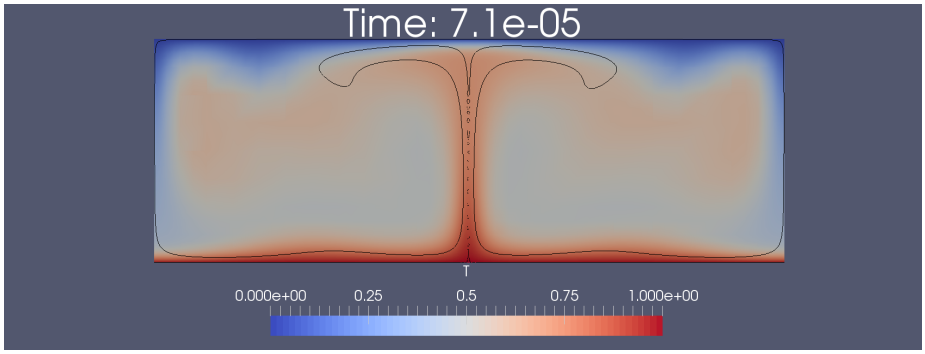

Figure 4: Convection problem showing interface reconstruction algorithm resolving sub-mesh scale features as 'bubbles'

One of the design benefits of the VoF method is the ability of the generated interface to fragment without need for costly and complex special coding. As can be seen in figure 4., the reconstruction algorithm has resolved a feature with an effective scale too small to have a definite form as a series of disconnected fluid regions rather than a connected stream due to beginning with the assumption of a connected local region. This is a smaller scale loss of accuracy than would be expected with any code which did not include interface tracking, though it may be one possible case for comparison when considering reconstruction algorithms.

$\eta = \eta_0$

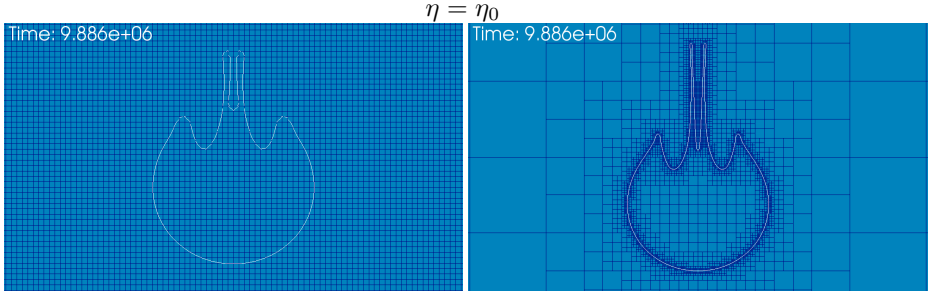

(a) Uniform 128x128 mesh

(b) AMR with maximum resolution of 512x512

Figure 5: Comparison of results for the falling block problem with constant viscosity showing the mesh and the reconstructed interface (white contour)

The second problem is a standard benchmark in the field [2], the 'Falling

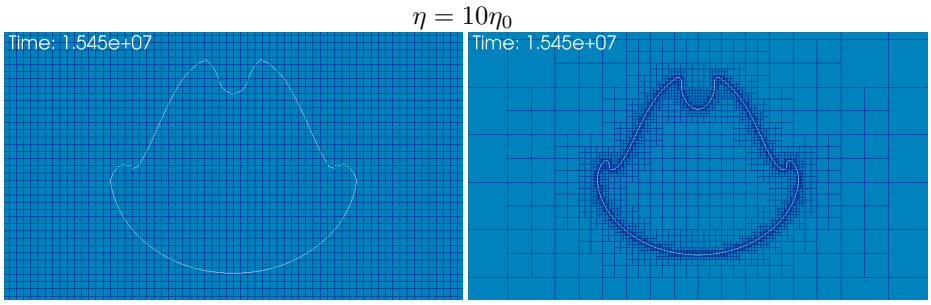

(a) Uniform 128x128 mesh

(b) AMR with maximum resolution of 512x512

Figure 6: Comparison of results for the falling block problem with constant viscosity showing the mesh and the reconstructed interface (white contour)

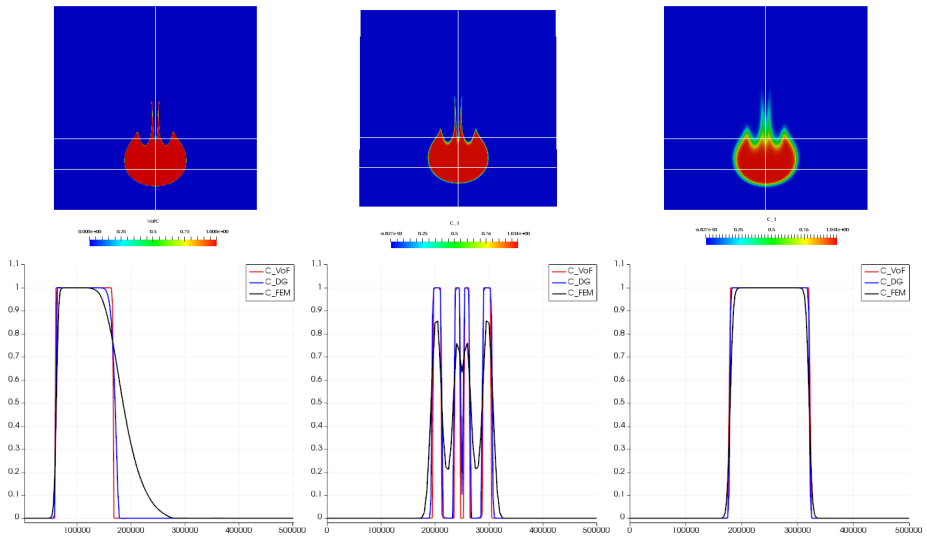

Figure 7: Comparison between VoF (left), Bounded Discontinuous Galerkin [3] (middle), and FEM Advection method in ASPECT (right)

Box' problem. For this problem, an initially square fluid volume with density $\rho = 3.3 \cdot 10^3$ and viscosity η sinks through a background fluid of density $\rho_0 = 3.2 \cdot 10^3$ and viscosity $\eta_0 = 10^{21}$. The results at the final timestep for $\eta = \eta_0$ and $\eta = 10\eta_0$ for uniform meshes are shown in figures 5a and 6a. Visual comparison shows similar final structures to the tracer particle methods in [2]. Note that although in the figures on the left there is some rounding of sharp corners as a result of the underresolution, the equivalent AMR tests with a maximum resolution equivalent to a 512x512 mesh in figures 5b and 6b do not exhibit this numerical artifact. Examination reveals a much better match to the tracer approximations in the [2]. A comparsion to other methods for modeling this problem available in ASPECT is shown in figure 7.

The final test problem is related to an active area of research. Heterogeneous compositional mantle models are frequently invoked to explain some observations obtained from geochemistry and seismology. In particular, two regions in the Earth's lower mantle, under the Pacific and Africa, are often interpreted as being piles of dense material, known as Large Low-Shear-Velocity Provinces (LLSVPs). In collaboration with Professors Billen, Kellogg, and Turcotte we are currently engaged in a research project to numerically model the thermochemical convection of a two-layer, density stratified region in which each of the materials obeys equations 1, 2 and 4. The particular configuration was initialized with the division between the composition at $z = \frac{d}{2}$, a full depth Rayleigh number of $R_a \approx 10^5$, and initial perturbations limited to boundary layers of size $\frac{d}{10}$, where d is the height of the domain. The tests were run for varying values of the nondimensional Bouyancy parameter $B = \frac{\Delta\rho}{\rho_0 \alpha \Delta T}$, with varying initial temperature perturbations. After a parameter survey, it was found that for a particular parameter space, the change from stratified to full depth convection did not take place until the interface between the two fluids showed some initial perturbation, so the initial conditions were adjusted to permit the addition of an initial perturbation to the fluid interface. Due to the scale of the behaviour of interest and the number of test runs necessary, a relatively coarse mesh of size 96x32 was used. The results of the test run are given in figures 8a and 9a for two interesting values of B. Figures 8 and 9 contain a comparison between the experiments of Davaille [1] and our computations for both stratified convection (figure 9) and full depth convection (figure 8) regimes. Note that despite the long time and expected high flow rate near the composition boundary, there is very little variation in the reconstructed interface for the case in the stratified region. Similarly, as is the design goal, the interface remains quite sharp in the case of the full depth convection mode. For the stratified region, a comparison to data from Davaille [1] descibing the temperature as a function of depth is shown in figure 10.

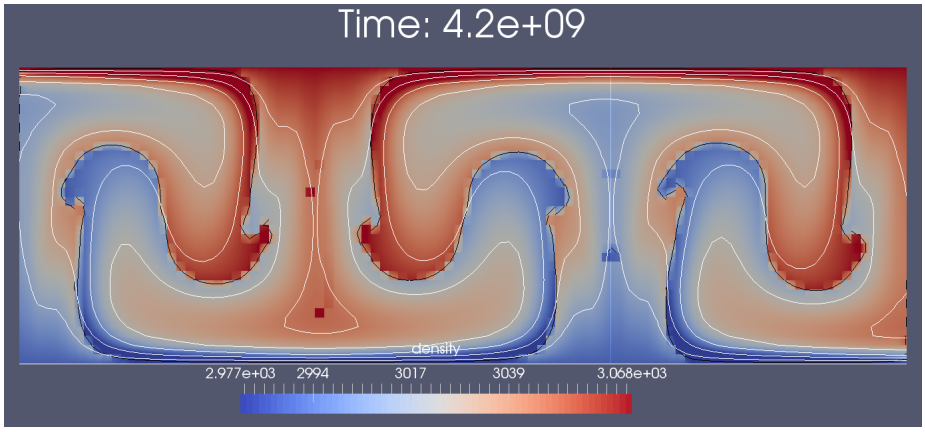

(a) Density colormap with temperature contours(white) and reconstructed interface(black) superimposed for model with $B = 0.4$

(b) Full depth convection from experiment ($B = R_\rho = 0.2$) by Dav Davaille [from 1, Fig1b]

Figure 8: Comparison of full depth convection model to experiment by Davaille [1]

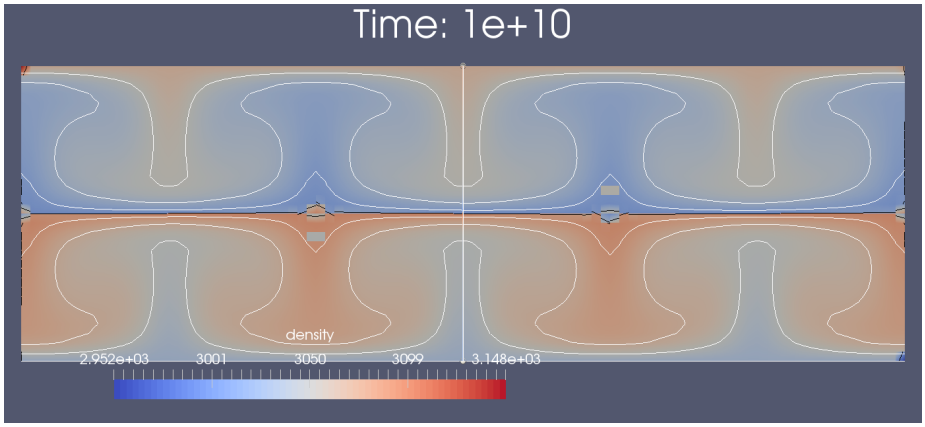

(a) Density colormap with temperature contours(white) and reconstructed interface(black) superimposed for model with $B = 0.7$

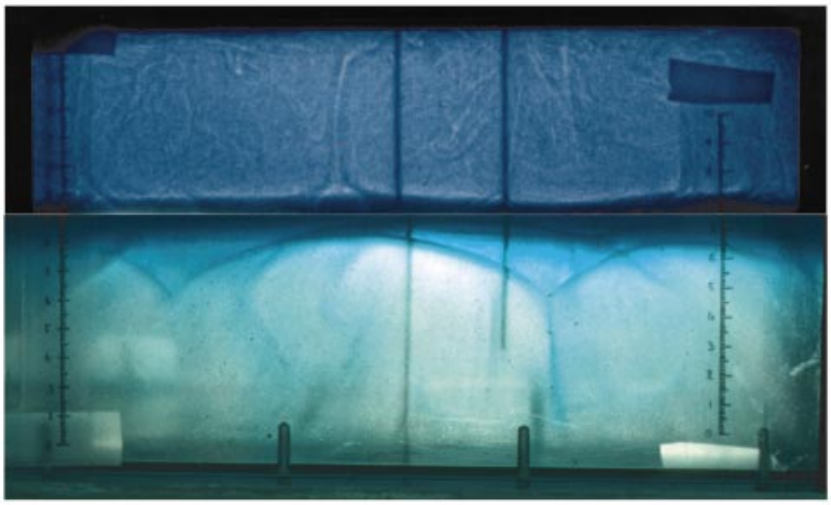

(b) Stratified convection from experiment ($B = R_\rho = 2.4$) by Davaille [from 1, Fig1f]

Figure 9: Comparison of stratified convection model to experiment by Davaille [1]

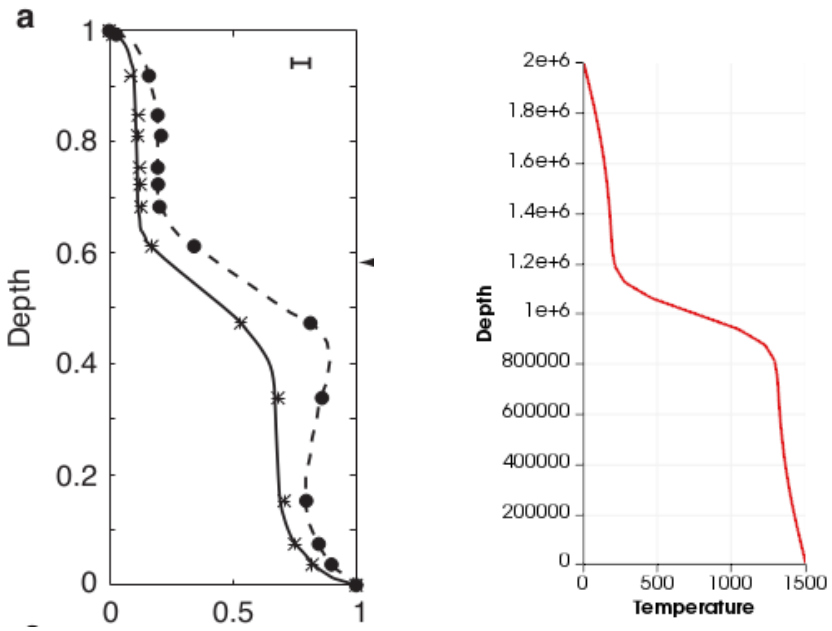

(a) Stratified convection from experiment ($B = R_\rho = 2.4$) by Davaille [1, Fig 1a]

(b) Stratified convection from VoF model ($B = 0.7$)

Figure 10: Comparsion of upwelling temperature-depth plots to experimental temperature-depth plots from Davaille [1]. Note: These are preliminary results and no attempt has been made to match the experimental values of the bouyancy parameter B, viscosity ratio γ, and depth ratio $\frac{d_2}{d1}$.

6 Future Work

- Implementation of a 3D interface reconstruction, and use of the 3D formulas for volume frction and interface location in Scardovelli [8] would allow the examination of the behavior of 3D systems.
- Improve volume fraction calculation to permit use of non-parallelogram meshes.
- Examination of other interface reconstruction approaches, such as the moment of fluid algorithm that allows the tracking of multiple materials.
- Examination of alternate advection algorithms; i.e. for flux fraction calculation to the donor region approach commonly used. This is likely to require significant additional information.

References

[1] Anne Davaille. "Simultaneous generation of hotspots and superswells by convection in a heterogeneous planetary mantle". In: *Nature* 402.6763 (Dec. 1999), pp. 756–760. DOI: 10.1038/45461. URL: http://dx.doi.org/10.1038/45461.

[2] Taras V. Gerya and David A. Yuen. "Characteristics-based marker-in-cell method with conservative finite-differences schemes for modeling geological flows with strongly variable transport properties". In: *Physics of the Earth and Planetary Interiors* 140.4 (2003), pp. 293–318. ISSN: 0031-9201. DOI: http://dx.doi.org/10.1016/j.pepi.2003.09.006. URL: http://www.sciencedirect.com/science/article/pii/S0031920103001900.

[3] Ying He, Elbridge Gerry Puckett, and Magali I. Billen. "A Discontinuous Galerkin Method with a Bound Preserving Limiter for the Advection of non-Diffusive Fields in Solid Earth Geodynamics". In: *Physics of the Earth and Planetary Interiors (submitted)* (2016).

[4] M. Kronbichler, T. Heister, and W. Bangerth. "High Accuracy Mantle Convection Simulation through Modern Numerical Methods". In: *Geophysics Journal International* 191 (2012), pp. 12–29.

[5] James Edward Pilliod. "An Analysis of Piecewise Linear Interface Reconstruction Algorithms for Volume-of-Fluid Methods". MS Thesis. Graduate Group in Applied Mathematics, University of California, Davis, Sept. 1992.

[6] James Edward Pilliod and Elbridge Gerry Puckett. "Second-order accurate volume-of-fluid algorithms for tracking material interfaces". In: *Journal of Computational Physics* 199.2 (2004), pp. 465–502. ISSN: 0021-9991. DOI: http://dx.doi.org/10.1016/j.jcp.2003.12.023. URL: http://www.sciencedirect.com/science/article/pii/S0021999104000920.

[7] Elbridge Gerry Puckett. "A volume-of-fluid interface tracking algorithm with applications to computing shock wave refraction". In: *Proceedings of the Fourth International Symposium on Computational Fluid Dynamics*. 1991, pp. 933–938.

[8] Ruben Scardovelli and Stephane Zaleski. "Analytical Relations Connecting Linear Interfaces and Volume Fractions in Rectangular Grids". In: *Journal of Computational Physics* 164.1 (2000), pp. 228–237. ISSN: 0021-9991. DOI: http://dx.doi.org/10.1006/jcph.2000.6567. URL: http://www.sciencedirect.com/science/article/pii/S0021999100965677.

[9] J. A. Sethian. *Level Set Methods and Fast Marching Methods*. 2nd. Cambridge University Press, 1999.

[10] Donald Turcotte and Gerald Schubert. *Geodynamics*. 3rd. Cambridge University Press, 2014.

Proposed Exam Syllabus

- Fluid Dynamics
  - Derivation of the Incompressible Euler Equations
    - Conservation of Mass
    - Conservation of Momentum
  - Rayleigh-Bernard Equations/Mantle convection
    - Incompressible Stokes Equations
    - Temperature Advection/Diffusion Equation
    - Boussinesq approximation
  - Nondimensionalization of the Stokes Equations
  - References:
    - Alexandre J. Chorin and Jerrold E. Marsden. *A Mathematical Introduction to Fluid Mechanics*. Springer New York, 1993. DOI: 10.1007/978-1-4612-0883-9. URL: http://dx.doi.org/10.1007/978-1-4612-0883-9
    - Donald Turcotte and Gerald Schubert. *Geodynamics*. 3rd. Cambridge University Press, 2014
- Finite Difference Methods
  - Stability of Explicit Finite Difference Methods for the 1D Advection Equation
  - Consistency of Explicit Finite Difference Methods for the 1D Advection Equation
  - Lax Equivalence Theorem
  - Godunov's Theorem and implications
  - Slope Limiters (Eg Minmax, Van-Leer)
  - Flux Corrected Transport
  - References:
    - Randall J. LeVeque. *Numerical Methods for Conservation Laws*. Springer Science + Business Media, 1992. DOI: 10.1007/978-3-0348-8629-1. URL: http://dx.doi.org/10.1007/978-3-0348-8629-1
- Finite Element Methods
  - Derivation of the Galerkin Method for Q1 on a 1D Uniform Mesh (eg for Heat Equation)
  - References:
    - Fish and Belytschko, A First Course in Finite Elements

- Numerical Methods in Linear Algebra
  - Jacobi Iteration
  - Gauss-Seidel Iteration
  - Multigrid
    - V-cycle
    - W-cycle
    - Full multigrid
  - Conjugate Gradient method
  - References:
    - William L. Briggs, Van Emden Henson, and Steve F. McCormick. *A Multigrid Tutorial, Second Edition*. Society for Industrial & Applied Mathematics (SIAM), Jan. 2000. DOI: 10.1137/1.9780898719505. URL: http://dx.doi.org/10.1137/1.9780898719505
    - Richard Barrett et al. *Templates for the Solution of Linear Systems: Building Blocks for Iterative Methods*. Society for Industrial & Applied Mathematics (SIAM), Jan. 1994. DOI: 10.1137/1.9781611971538. URL: http://dx.doi.org/10.1137/1.9781611971538